Cancer Medicine

WILEY

Cancer Medicine Open Access

RESEARCH ARTICLE OPEN ACCESS

Bone Marrow Failure Model Mimics Aplastic Anemia Patients: Single-Cell Landscape of Immune Response Reveals Novel Mechanisms of Immune Imbalance in AA

Shuai Tan | Fang Fang | Jing Sun | Yumeng Li | Yaochi Chen | Wanling Sun

Department of Hematology, Xuanwu Hospital, Capital Medical University, Beijing, China

Correspondence: Wanling Sun (wanlingsun@xwhosp.org)

Received: 26 November 2025 | **Revised:** 8 May 2026 | **Accepted:** 14 May 2026

Keywords: aplastic anemia | bone marrow failure | immune cells | platelet | single-cell sequencing

ABSTRACT

Background: The pathogenesis of HSPCs impairment in aplastic anemia (AA) remains unclear. We focused on $CD8^+$ T cells and investigated platelets, $CD4^+$ T cells, macrophages, and mitochondrial energy metabolism, aiming to elucidate the cellular atlas changes associated with bone marrow failure (BMF).

Methods: We have successfully established a mouse model of bone marrow failure and analyzed the immune response at the single-cell level.

Results: Platelets regulate $CD4^+$/$CD8^+$ T cells and macrophages by releasing PF4. CXCR3/CXCR5 bind to PF4, activating mitochondrial signaling pathways. The decrease of Treg weakens immunosuppression. Additionally, there is a significant increase in $CD8^+$ effector T cells. Increased energy metabolism was observed in $CD8^+$ stress T cells. It should be noted that platelet reduction itself in AA weakens energy metabolism, subsequently impairing the hemostatic and thrombotic functions. However, platelets' regulatory function in immune cells remains significant. An imbalance in M1 and M2 macrophage polarization is observed. While a phenotype macrophage and $CD8^+$ naive T cells are important cell phenotypes in marrow aging, they do not contribute to pathology failure.

Conclusion: The possible mechanisms of BMF in AA: based on PF4, platelet-T cell/macrophage crosstalk leads to immune overactivation and the release of cytokines such as IFN-γ and TNF-α, which attack the marrow. Therefore, transforming imbalanced $CD8^+$ effector T cells, stress T cells, Treg cells, and M1/M2 macrophages into $CD8^+$ naive T cells and a phenotype of macrophages via inhibiting platelet immune regulatory function may provide a promising strategy to reverse BMF.

1 | Introduction

AA is an acquired and immune-mediated bone marrow failure disease characterized by cytopenia and hypocellular bone marrow [1]. Due to the empty BM, researchers can only acquire a paucity of bone marrow cells. It remains challenging to explore the pathogenesis of AA [2, 3].

To overcome the scarcity of bone marrow cells from patients with AA, an immune-mediated BMF murine model has been established [4]. B6D2F1 mice as a recipient (cross between C57BL/6 female and DBA/2 male) are given TBI followed by LN cells infusion intravenously from parental C57BL/6 donors. Due to the mismatched MHC molecular, the LN cells from donor mice were activated, and the HSPC cells in

Shuai Tan and Fang Fang contributed equally.

This is an open access article under the terms of the Creative Commons Attribution-NonCommercial License, which permits use, distribution and reproduction in any medium, provided the original work is properly cited and is not used for commercial purposes.

© 2026 The Author(s). *Cancer Medicine* published by John Wiley & Sons Ltd.

recipient mice were destroyed, resulting in severe pancytopenia and BMF. This model replicated the pathologic process of human AA. The increasing evidence supports that the inflammatory cytokine contributes to AA development, but the detailed understanding of inflammatory signaling in AA is still on the way.

With high throughput single-cell techniques adopted, such as single-cell sequence and single-cell mass cytometry (cytometry by time-of-flight, CyTOF), the insights into the pathophysiology of AA have been further widened [5]. Recently, a single-cell transcriptomics study revealed that in $CD8^+$ effector and memory T cells, genes associated with cytokine production, activation, and exhaustion have been up-regulated. Meanwhile, the cell death signal has been enriched in $CD4^+$ naïve and memory T cells. These might be responsible for the inversion of the CD4:CD8 ratio and the reduced quantity of $CD4^+$ T cells [6].

Apart from activated pro-inflammatory factors, the immune regulatory factors have been suppressed in AA. Recently, studies revealed that the percentage and the absolute number of NK cells were reduced in patients with AA [7, 8]. The bone marrow NK cells from AA patients had a stronger immune regulatory function and exhibited a diminished INF-γ production which suggests a diminished NK cell function [7]. The Treg subset has a robust immunosuppressive activity, but it has been reported that a $CD30^+$ Treg population in AA patients was decreased [9]. The above studies suggest that overproduction of pro-inflammatory cytokine, imbalanced immune cell subset, and especially autoreactive T cell destruction of HSPCs are thought to be major culprits in the pathogenesis of AA, but previous studies still have limitations. The immune network is complex, but most studies focus on specific cell types. The mechanism of how the immune cytokine and immune cells cooperate, contributing to disease progression is unknown.

In addition, platelets are traditionally seen as crucial players in hemostasis, coagulation, and maintaining the integrity of the vascular endothelium. Accumulating evidence supports that platelets also play a significant role in immune response [10]. When the $CD4^+$T cell and autologous platelets were co-cultured, the platelets promoted cytokine secretion and further regulated $CD4^+$ T cell differentiation [11]. Moreover, PF4, a platelet-derived mediator, can enhance $CD4^+$T effector memory cell response through the mitochondrial-Akt-PGC1α-TFAM pathway [12]. Typically, in single-cell sequencing studies, platelets and mitochondria are discarded as cell debris during the preparation phase [13]. In our study, we retained platelets and mitochondria during preparation and tried to clarify whether platelets participated in immune interaction in AA.

In a mouse model of bone marrow failure, single-cell RNA-seq was used for the first time to thoroughly analyze the connections between various immune cell populations. Especially, it revealed that in the BMF model, platelets can regulate the immune response of $CD8^+$ and $CD4^+$ T cells through mitochondrial metabolic pathways. Aging is also viewed as a chronic inflammation process. An aging mouse was included as control in this study, which would be beneficial for deciphering the differences in inflammation at physiological and pathological levels. This study allows for a more comprehensive understanding of the immune interactions and metabolic processes in AA.

2 | STAR Methods

2.1 | Method Details

2.1.1 | Animal Grouping and Ethics Statement

For a total of four samples, each comprising a single mouse, this work used high-throughput single-cell sequencing, treating each experimental group as an independent sample. Complete blood counts and body weight analyses were carried out separately in the TBI group ($n=3$) and the BMF group ($n=4$), despite the small sample size. The sample design was meant to produce preliminary, testable hypotheses rather than to support large-scale statistical inference because the goal of this study was to investigate novel pathogenetic pathways. The mice were divided into four groups: the BMF group (experimental group), the whole-body irradiation (TBI) group (control group), the normal young mouse group (WT), and the normal aged mouse group (Aged). Specifically, first-generation hybrid B6D2F1 mice were bred by crossing C57BL/6 and DBA/2 mice. These male mice, aged 8–12 weeks, were used as test subjects for the BMF mouse model. Male C57BL/6 mice, aged 8–12 weeks, were used as lymphocyte donors. Male B6D2F1 mice, aged 8 weeks, served as the normal young mouse group, while male B6D2F1 mice, aged 104 weeks, served as the normal aged mouse group. All mice were provided by Beijing Weitong Lihua Experimental Animal Technology Co. Ltd. and were housed in a standard highly hygienic environment. The study was approved by the Experimental Animal Welfare Ethics Committee of Xuanwu Hospital, Capital Medical University (approval number: XW-20210531-1).

2.1.2 | BMF Mouse Model

Recipient B6D2F1 mice were randomly assigned to either the Total Body Irradiation (TBI) group or the BMF group. Lymphocyte suspensions were prepared by collecting cervical, axillary, mesenteric, and inguinal lymph nodes from the C57BL/6 mice. The lymph nodes were ground and filtered through a 70 μm cell filter. Both the TBI group and the BMF group of B6D2F1 mice received 5.0 Gy TBI. Four hours post-irradiation, mice in the BMF group were injected intravenously with 4×10^6 lymphocytes from C57BL/6N mice via the tail vein. After the lymphocyte infusion, the mice exhibited symptoms such as hunched backs, weight loss, disheveled fur, and reduced activity from Day 9 to Day 14. Mouse samples were collected after the 10th day of the study [14, 15].

2.1.3 | Peripheral Blood Routine Test

Blood samples were collected from the tail vein of mice in both the TBI and BMF groups into EP tubes containing ethylenediaminetetraacetic acid (EDTA) as an anticoagulant. The samples were placed on ice for processing. The levels of white blood cells,

hemoglobin, and platelets were measured using an automated blood cell counter.

2.1.4 | Bone Marrow Examination (Sternal Immunohistochemistry and Pathological Staining)

Bone marrow samples were collected from all four groups, with each group providing four samples. The mouse sternums were isolated and fixed in centrifuge tubes containing 4% paraformaldehyde. After decalcification, the sternums were embedded in paraffin, and sections were dewaxed, rinsed with water, and subjected to antigen retrieval. Sections were blocked with 3% bovine serum albumin at room temperature for 30 min. Primary antibodies against CD68, F4/80, CD86, CD206, and CD163 were added dropwise, and the sections were incubated overnight at 4°C in a wet box. After three washes with phosphate-buffered saline, the secondary antibody was incubated at room temperature for 50 min. Diaminobenzidine was used to promote coloration, and the sections were dehydrated and mounted after counterstaining the nuclei with hematoxylin. Hematoxylin–eosin staining was used for pathological analysis. Histological characteristics of the bone marrow from the two groups were observed under an optical microscope.

2.1.5 | Single-Cell Solution Preparation

Bone marrow was dissected into 1–2 mm pieces and digested using the SoloTM Tumor Dissociation Kit (Sinotech Genomics, JZ-SC-58201) at 37°C for 30–60 min. Enzymatic digestion was stopped by adding excess RPMI-1640 medium, and the cell suspension was filtered through a 40 μm cell strainer. The resulting single-cell solution was kept on ice before being loaded onto the BD Rhapsody cartridge for single-cell transcriptome capture.

2.1.6 | Single-Cell Transcriptome Capture, Library Construction, and Sequencing

Cells were first stained with two fluorescent dyes, Calcein AM and Draq7, to precisely determine cell concentration and viability using the BD Rhapsody Scanner (BD Biosciences) before antibody-based labeling. Each sample was stained for 30 min on ice with 25 AbSeq antibodies targeting major mouse immune markers from the BD Abseq immune discovery panel (Cat. No. 940320, 940,107, 940,110, 940,119, 940,132, 940,130, 940,127, 940,168, 940,109, 940,163, 940,131, 940,108, 940,345, 940,137, 940,417, 940,116, 940,496, 940,329, 940,357, 940,437, 940,128, 940,134, 940,165, 940,209, 940,151). Afterward, the cells were labeled with the respective AbSeq antibodies, washed three times with Stain Buffer (FBS) (BD Biosciences, Cat. No. 554656), and loaded into a BD Rhapsody micro-well cartridge for single-cell capture.

Excessive cell capture beads were added to ensure nearly every micro-well contained a bead, and any excess beads were washed away. After cell lysis with lysis buffer, cell capture beads were retrieved, washed, and reverse transcription was performed. The microbeads captured single-cell transcriptomes, along with Ab-tagged index sequences targeting 25 immune cell-associated surface antigens, generating separate cDNA libraries for transcriptome and AbSeq, each containing cell labels and unique molecular identifier (UMI) information. The entire process followed the manufacturer's protocols using the BD Rhapsody cDNA Kit (BD Biosciences, Cat. No. 633773) and the BD Rhapsody WTA Amplification Kit (BD Biosciences, Cat No. 633802). The libraries were sequenced using the PE150 mode (Pair-End for 150 bp read) on the NovaSeq 6000 platform (Illumina).

2.1.7 | Data Pre-Processing and Quality Control

The BD pipeline filtered feature/barcode tables were processed with a custom script to create a Seurat object (Seurat package, v4.3.1) [16]. To recover platelets from the BD raw data, the top 5000 droplets with the most detected genes were extracted from the original BAM file for each sample, and all droplets were merged for further processing. The following steps were implemented to retain platelet-size droplets:

MK/Platelet-related signature genes were obtained from the "m5.go.bp.v2023.1.Mm.symbols.gmt" file, and for each droplet, a "MKPP score" was calculated using the Seurat function "AddModuleScore." A "cell-to-mean correlation" metric was then calculated, following the approach described in the paper (DOI: 10.1186/s13059-016-0888-1), to distinguish real cells from empty droplets. Based on the distribution of these two metrics, the top 25% MKPP-scoring droplets with a cell-to-mean correlation greater than 0.3 were retained for further integration with the BD-filtered dataset. The resulting cells were considered valid and used for subsequent analysis.

2.2 | Cell-Type Identification and Sub-Clustering Analysis

In this study, AbSeq was employed to co-detect RNA and protein expression for each cell. To perform multi-modal cell clustering and annotation of major cell types, we used MOFA to integrate the RNA and protein data. Initially, the read counts from both RNA and protein data were separately normalized across all cells. The RNA data were normalized using the default parameters of Seurat's "NormalizeData" function, while protein data underwent centered log-ratio transformation. The normalized data were then used to select highly variable genes (HVGs) for the RNA data using Seurat's "FindVariableFeatures" function (selection.method = "mvp"). Next, two matrices were created: one for the top 3500 HVGs from the RNA data and another for all 20 proteins from the protein data. These matrices were used to create a MOFA object.

Factors and weights extracted from the MOFA results were used as integrated multi-omic representations in latent space. The first 26 factors were selected for downstream analysis. We then used the "FindNeighbors" and "FindClusters" functions to identify clusters of expression-similar cells, with an empirically set resolution of 0.5. The "RunUMAP" function was applied for data visualization. Differentially expressed genes (DEGs) for each cluster, compared to the remaining clusters, were identified using the "FindAllMarkers" function. To annotate the cell

identities of the clusters, we curated a list of canonical gene markers for 17 major cell types. These markers included genes such as 'Cd34', 'Kit' for HSC/MPP; 'Gypa', 'Hemgn' for EP; 'Dntt', 'Igll1' for CLP; and others for specific cell types like B cells, plasma cells, macrophages, neutrophils, and T/NK cells. A cluster was assigned a canonical identity based on expression enrichment of the marker genes.

2.3 | Sub-Clustering Analysis

For sub-clustering analysis, we applied the same workflow to the progenitor population (HSPCs) and four mature cell types: Macrophages, Neutrophils, T/NK cells, and B cells. For each cell type, the extracted cell subsets were processed in the same manner as the global map. Clustering was performed at resolutions ranging from 0.1 to 0.5, with increments of 0.05. One of the resolutions was selected for downstream analysis. Marker genes were determined for each subset using the same method applied in the global cluster analysis with default settings.

2.4 | Identification of Differentially Expressed Genes (DEGs) and Pathway Enrichment

To identify inter-group DEGs, the Seurat function "FindMarkers" was used to calculate the differences between the compared groups using a *t*-test model. Genes were filtered based on a minimum fold change of 0.25 (avg_logFC) and a maximum *p*-value of 0.05 (*p*_val). Gene Ontology Biological Process (GOBP) enrichment analysis was performed using the "enrichGO" function from the clusterProfiler (v3.14.3) package. Additionally, we conducted Reactome pathway enrichment based on the DEGs from different cell types and diseases using the "GSEA" function. The GSEA model "fgsea" was used on gene sets containing between 15 and 500 genes, and sorted genes were tested for enrichment in Reactome pathways from MsigDB. Pathways with a Benjamini-Hochberg corrected two-sided p-value < 0.05 were considered robust and used for further analysis.

2.5 | Enrichment Score Analysis of Functional Processes

Enrichment scores for each cell in the targeted cell population were estimated using the Seurat function "AddModuleScore" with a list of reference signature genes. These included genes associated with various functional processes such as PhosphoAkt (GO: 0043491), AMPK (GO: 2000479), JAK (GO: 0007259), ROS (GO: 1903409), ATP (GO: 0042773), and MAPK (GO: 0000165), as well as hallmark gene sets like IFN-γR (HALLMARK_INTERFERON_GAMMA_RESPONSE), BIOCARTA_NFKB_PATHWAY, HALLMARK_P53_PATHWAY, TFAM_TARGET_GENES, and BIOCARTA_PGC1A_PATHWAY. Additionally, classical M1 and M2 macrophage markers were used (M1: "Nos2", "Cd86", "Cd80", "Cd38", "Fcgr3", "Fcgr2b", "Il1b", "Il6", "Il12a", "Il12b", "Il23a", "Tnf"; M2: "Cd163", "Mrc1", "Il10", "Arg1", "Chil3", "Retnla", "Tfrc", "Tgfb1", "Vegfa", "Slc40a1", "Nfe2l2", "Hmox1"). Each enrichment score was generated by calculating the total gene expression for each of the analyzed genes and separating them into 25 classifications of similar expression levels. For each gene in a target signature, 100 "control" genes were selected from the corresponding category and added to the "control" gene set. This control gene set was constructed to match the expression distribution of the target signature, with its average representing an equivalent sampling of 100 genes of equal size to the target gene set. The expression of genes in the target and control sets was averaged among each cell, and the cell's score for the target gene set was calculated as the difference between the target and control scores.

2.6 | Cell–Cell Interaction (CCI) Analysis

Cell–cell interactions (CCI) between assigned cell populations from different groups (combinations of WT, TBI, BMF, and Aged) were inferred using CellChat (version 1.1.3) [17]. The CellChat database (CellChatDB) was used to analyze CCI. Log-transformed, normalized gene counts were utilized by default for CCI analysis. Data from the different groups were fed into the CCI analysis workflow, and a merged data object was created using the "mergeCellChat()" function for further identification of significant CCI changes between the compared groups. The functions "compareInteractions()" and "netVisual_diffInteraction()" were used to compare aggregated communication probabilities between the groups. The "rankNet()" function was applied to generate interaction bar plots for information flow. Circle plots were generated showing pathway-specific changes in interaction strength between cell types by aggregating communication probabilities by cell type. Additionally, the "netVisual_aggregate()" function was used to create chord plots depicting cell type interactions for specific signaling pathways.

2.7 | Quantification and Statistical Analysis

GraphPad Prism 8.0 was used to analyze and visualize the hemoglobin, platelet, and white blood cell counts in the peripheral blood of mice in the TBI and BMF groups. The data are shown as mean ± standard deviation (mean ± SD). Unpaired *t*-tests were used to determine statistical significance between two groups, and one-way ANOVA was used to compare groups. A p-value of less than 0.05 was deemed statistically significant, and $p < 0.05$, $p < 0.01$, and $p < 0.001$ are indicators of statistical significance. The functions "DimPlot", "FeaturePlot", "DotPlot", and "VlnPlot" were used to reproduce all figures. Heatmaps were generated using the R package "ComplexHeatmap" (version 2.8.0).

3 | Results

3.1 | Based on PF4, Platelet-T Cell/NK Cell/Macrophage Crosstalk and Immune Imbalance Drivers in AA

In aged bone marrow, Treg cells and NK cells were decreased, and $CD8^+$ naive T cells account for the dominant population. The number of $CD4^+$ Tfh cells, Th, $CD8^+$ T cells (including $CD8^+$ naive T, $CD8^+$ effector T, $CD8^+$ Tem) increased, and the

mitochondrial metabolic level and number of $CD8^+$stress T cells are significantly enhanced. Macrophages, except for the type macrophage, increased significantly, with M1 macrophages being predominant. During aging, a special state of macrophages ($Pf4^{hi}$, $Cd68^{hi}$, $Timd4^{hi}$, $Apoc1^{hi}$, $S100a8/a9^{hi}$, $Cd163^{dim}$, $CD86^{dim}$, $C1qa^{dim}$) emerges, which occupies a dominant position in aging bone marrow. Treg cells release IL-10 and TGF-β; $CD4^+$ Tfh cells secrete IL-21, which in turn promotes the secretion of IFN-γ; $CD8^+$ Tem cells secrete IFN-γ; M1 macrophages release pro-inflammatory cytokines such as IFN-γ, TNF-α, and IL-β, attacking hematopoietic stem and progenitor cells, leading to an imbalance in the immune "balance seesaw" and ultimately resulting in BMF (Figure 1).

3.2 | Single-Cell Transcriptome Analysis of Bone Marrow Mononuclear Cells (BMMCs) in a Mouse Model of Bone Marrow Failure

To analyze the immune characteristics of various cells in AA at the single-cell level, we employed the "Single cell RNA-seq+ABseq" technique, integrating single-cell RNA-seq with antibody-based protein detection (WTA for whole-transcriptome amplification+ABseq for antibody sequencing). This method was used to investigate the transcriptome of four groups of mouse BMMCs: TBI (total body irradiation/control group), BMF (Bone Marrow Failure/experimental group), WT (wild type/normal young group), and Aged (normal elderly group). The schematic diagram of the study design and workflow is shown in Figure 2A. After modeling, we conducted quantitative and qualitative analysis of the mouse bone marrow. In the BMF group, the mice exhibited significant weight loss, graying of fur, hunched posture, reduced activity, and even death. Moreover, the hematopoietic area was significantly reduced, and levels of HGB, WBC, and PLT were markedly decreased. These findings suggest that the modeling was successful (Figure 2B,C).

Following rigorous bone marrow mononuclear cell (BMMC) filtration and quality control (see Methods), 17 distinct cell subtypes were found using UMAP-based dimensionality reduction and clustering (Figure 2D). The distribution and proportions of these 17 cell subtypes were compared between the four groups. The BMF group exhibited a significant decrease in total cell numbers, with the majority of the surviving cells being $CD8^+$T and $CD4^+$T cells, particularly $CD8^+$T cells. Additionally, the proportion of macrophages was significantly increased in the BMF group (Figure 2E,F). The expression of distinctive marker genes served as the basis for cluster categorization; Figure 2G,H displays exemplary expression patterns.

3.3 | In the BMF Model, There Was an Immune Imbalance Between $CD8^+$ T Cells and $CD4^+$ T Cells, Characterized by Enhanced Expression of the T Cell Membrane Receptor CXCR3

We sub-clustered and annotated T/NK cells in four groups based on marker gene expression (Figure 3A), dividing T cells into different subtypes. We assessed T/NK cell subsets distribution and found different T-cell subset compositions among the four groups (Figure 3B,C). The proportion of NK cells significantly decreased or even disappeared in BMF. The CD4/$CD8^+$ T cell ratio also decreased. In the expanded $CD8^+$ T cell subsets, effector T cells dominated, with naive T cells being notably reduced compared to other groups. In the BMF model, the total number of T cells was significantly increased, accompanied by an elevation in Tfh cells and a reduction in Treg cells.

In the control group (WT/TBI), the proportion of Tfhs was extremely low. In the Aged group, the proportion of $CD8^+$ T cells was significantly higher than that of $CD4^+$ T cells, but the proportion of naive $CD8^+$ T cells was significant. The proportion of Tregs in this group was significantly higher than in BMF.

Given the previously reported role of PF4 in modulating T cell function through CXCR3, we additionally examined CXCR5; we next examined the expression of CXCR3 (and CXCR5) across T cell subsets to explore their potential involvement (Figure 3D,E). CXCR3 was not expressed in NK, $CD4^+$ Treg, and $CD8^+$ naive T cells in the BMF group. Platelet-released PF4 can bind to the membrane receptor CXCR3, stimulating T cell immune responses and enhancing the Treg phenotype. However, in BMF, $CD4^+$ Treg did not express CXCR3, resulting in a decrease in Treg cells and causing immune imbalance. On the other hand, CXCR3 was highly expressed in other types of T cells. In contrast, it was mainly expressed in $CD4^+$ Treg and $CD8^+$ naive T cells in the Aged group. CXCR5 was not expressed in the control groups and was mainly expressed in $CD4^+$/$CD8^+$ TEM cells in the BMF group.

Additionally, we summarized the gene expression of these cells and enriched their functional pathways (Figure 3F,G). Further comparison of the upregulated expression of signaling pathways in these cells across the four groups (Figure 3H,I) revealed that, compared to the WT group, the BMF group showed upregulated functions related to T cell and lymphocyte differentiation. Compared to TBI, BMF had upregulated expression of functions related to innate immune response regulation in $CD4^+$ proliferative T cells, and upregulated expression of ribosome biosynthesis processes in $CD8^+$ naive T cells. In the Aged group, $CD8^+$ proliferative T cells and NK cells were more closely associated with the lymphocyte differentiation process.

3.4 | M1/M2 Imbalance in BMF and Emergence of Mph05 Macrophages in Aged Group

To explore the impact and role of macrophages in AA, we compared the proportions of five major macrophage types in BM across four groups (WT, TBI, BMF, Aged). Each group's cells are shown as individual UMAP plots (Figure 4A,B). Combined with the bar charts illustrating the proportions of various macrophage types (Figure 4C), we observed that in the BMF group, Mph05 constitutes a very small proportion, while the total number of macrophages is the highest in this group. Among them, the proportion of M1-type macrophages exceeds that of M2-type. In the control groups (WT/TBI), M2-type macrophages are much more abundant than M1-type. Conversely, in the Aged group, Mph05 accounts for nearly 100%. Additionally, this type of macrophage constitutes more than 75% in WT and nearly 50% in TBI. The Mph05 cells exist in both young and aged mouse bone marrow but do not cause disease.

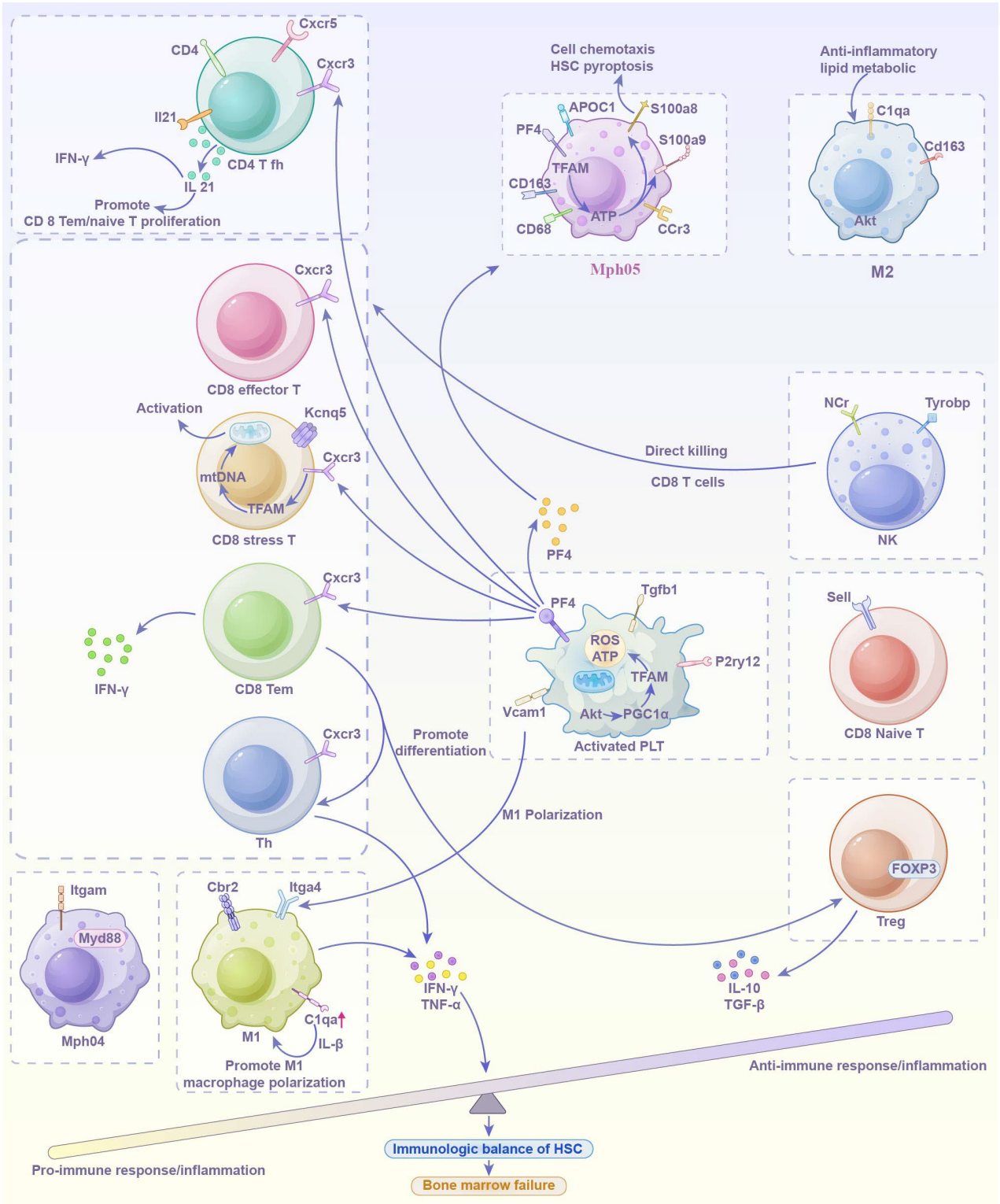

FIGURE 1 | Single-Cell Transcriptomic Dissection Analysis of Immunological Responses in the BMF Mouse Model: Based on PF4, Platelet-T cell/NK cell/Macrophage Crosstalk and Immune Imbalance Drivers in AA. The overall design adopts a "seesaw" format to illustrate the immune homeostasis imbalance in the BMF mouse model. Each cell is labeled with its highly expressed marker, with the left panel showing pro-inflammatory immune cell populations that are predominant, and the right panel showing reduced numbers of anti-inflammatory immune cells. In the middle, crosstalk between platelets and various immune cells is depicted to visualize the imbalance between pro- and anti-inflammatory responses (Figuredraw was used to draw this figure).

Clustering was annotated based on typical marker gene expression, with the scaled expression distribution of selected genes shown in Figure 4D–F. CD86, a representative marker of M1 macrophage polarization, is expressed more in the M2 group of cells. The phenotype of macrophage ($Pf4^{hi}$, $Cd68^{hi}$, $Timd4^{hi}$, $Apoc1^{hi}$, $S100a8/a9^{hi}$, $Cd163^{dim}$, $CD86^{dim}$, $C1qa^{dim}$). In addition

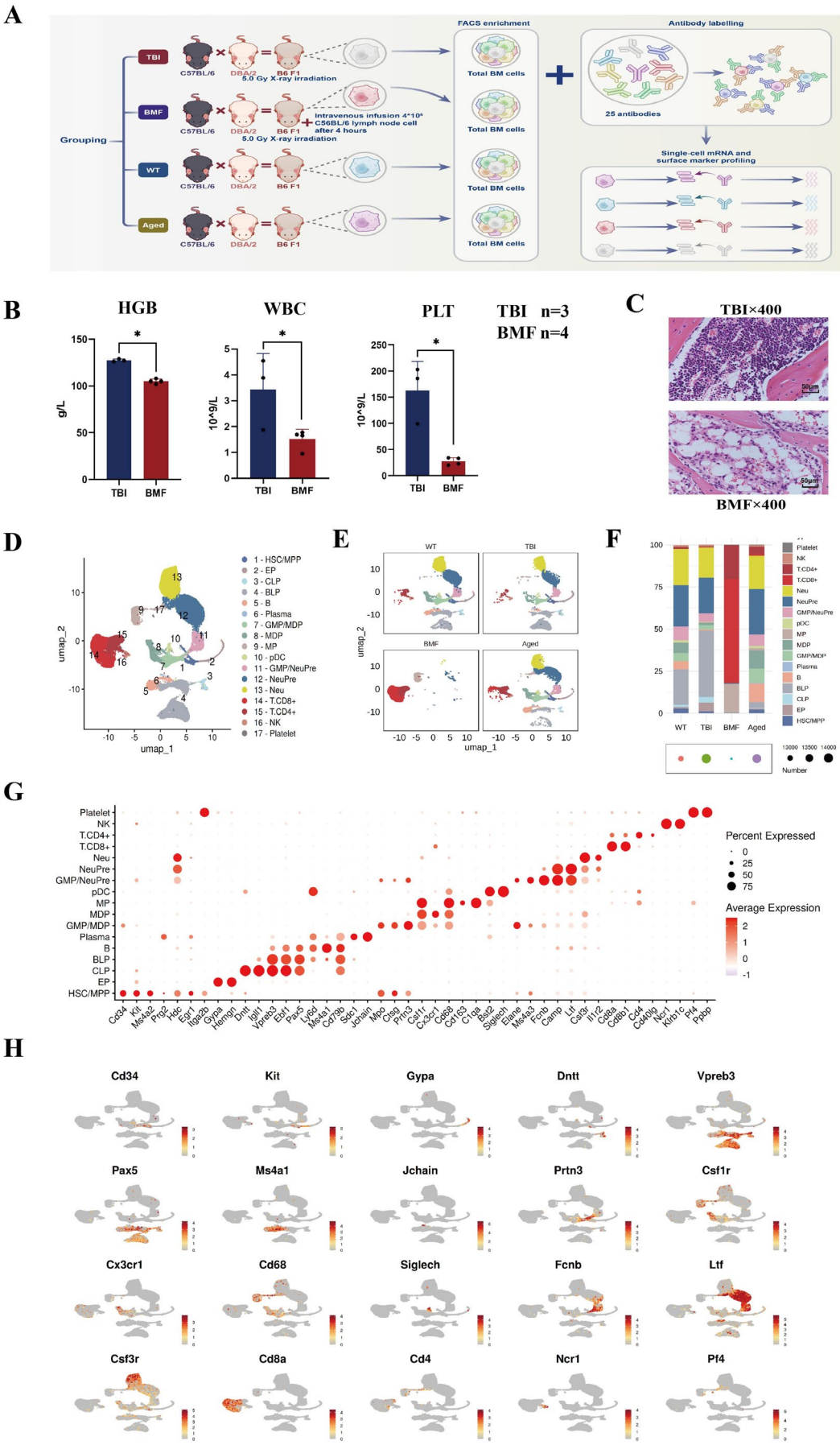

FIGURE 2 | Legend on next page.

FIGURE 2 | Single-cell Transcriptome Analysis of Bone Marrow Mononuclear Cells (BMMCs) in the BMF Mouse Model. (A) Schematic diagram of the study design and analysis workflow. BMMCs under four conditions were subjected to the "Single cell RNA-seq Workflow" (WTA (whole-transcriptome amplification) + ABseq (antibodyseq)), including four groups: TBI (total body irradiation, irradiation/control group), BMF (BMF, BMF/experimental group), WT (wild type, wild type/normal young group), and Aged (normal elderly group). The output data were used for expression analysis. (B) Hemoglobin (HGB), white blood cell (WBC), and platelet (PLT) counts in TBI and BMF mice are displayed as mean ± SD in bar graphs. A statistically significant difference between groups is shown by $p < 0.05$. (C) Bone marrow morphology of TBI and BMF groups (magnified 400 times). (D) UMAP plot showing 17 cell clusters. (E) UMAP plots showing different cell types in different groups. (F) Bar chart showing the proportion of cells of a specified cell type in different samples/groups. (G) Bubble heatmap showing marker genes in different types. The size of the dots represents the proportion of expressing cells, colored according to the normalized z-score expression level. (H) UMAP plot showing the expression distribution of marker genes.

to expressing common macrophage markers such as Cd163 and Cd68, they also express specific genes like Pf4 and Apoc1.

The gene C1qa is under-expressed in Mph04 and Mph05 cells. We also show that the M1 score in this group of cells is second only to Mph01, while the M2 score is second only to Mph02 (Figure 4G). This suggests that the polarized cell type in this group may be Mph05 macrophage, which could possess characteristics of both M1 and M2 cells.

We performed comprehensive enrichment analysis to explore the transcriptional features of these macrophage subtypes (Figure 4H). M1 macrophages are associated with promoting inflammation, M2 macrophages play an anti-inflammatory role in lipid metabolism, and M4 macrophages are linked to cell chemotaxis. In summary, we propose to term this type of macrophage, derived from the aging and osteopenia process, detailed explanations will be provided in the subsequent discussion section.

3.5 | In BMF, the Crosstalk Between Platelets, T Cells, and Macrophages Is Enhanced

Platelet-specific gene Pf4 predominantly exhibits high expression in platelets among various cell types (Figure 5). Dimensionality reduction results (Figure 5A–C) show that in the Aged group, Pf4 expression is high only in platelet cell types. Additionally, the genes Tgfb1 and P2ry12 are also highly expressed in platelets. A deeper exploration of the interaction strength between platelets and various cells (Figure 5D–F) revealed that in the BMF group, when platelets acted as receptors, the association with MP was most significantly upregulated. Further analysis revealed the enrichment of specific signaling pathways in platelets across various groups (Figure 5G): PGC1α, AMPK, and Akt signaling pathway proteins were highly expressed in platelets from the Aged group but were weaker in the BMF group.

3.6 | Pseudotime Analysis of T Cells and Macrophages

We further delineated the distribution trajectories of T cells, macrophages, and specific genes along the pseudotime axis in different groups. Treg cells were mainly at the end of the aged group's trajectory, while $CD4^+$ Tfh and $CD8^+$ effector T cells spanned the entire BMF trajectory but were sparse in the aged group (Figure 6A,C). Three T cell gene clusters peaked in the early, middle, and late phases (Figure 6B). CXCR3 expression peaked over time in the BMF group (Figure 6D). M1 and M2 macrophages were concentrated in the BMF group (higher M1 than M2), while the type macrophage was in the early and late phases of the aged group (Figure 6E,G). Three macrophage gene clusters peaked in the late, early, and middle phases (Figure 6F). PGC1α and TFAM mitochondrial pathway proteins showed no significant temporal changes and were mainly expressed in the BMF group.

3.7 | During BMF, Platelets Release PF4, Which Interacts/Crosstalks With T Cells and Macrophages

Using CellChat (version 1.1.3), we determined CCIs between the specified 17 cell populations across different comparisons (combinations of WT, TBI, BMF, Aged). In the BMF group, ligand-receptor pairs were observed between PLT and itself, MDP, MP, NeuPre, $CD4^+$ and $CD8^+$ T cells. Notably, the number of ligand-receptor pairs between MP and itself was the highest in this group (Figure 7A).

A circular diagram was generated to show pathway-specific changes in interaction strength between cell types by summarizing communication probabilities (Figure 7B–G). The ligand-receptor interaction analysis revealed that in the BMF group, whether MP provided ligands or receptors, it had close connections with T cells, NeuPre, and MDP. When MP provided ligands, its interaction with platelets was weaker compared to when it acted as a receptor, and the interaction between MP and platelets weakened further in the Aged group. The connection between NK and various cells weakened, and a strong ligand-receptor relationship between NK and MP was observed in both $CD4^+$ and $CD8^+$ T cells.

Using the netVisual aggregate function to display the chord diagram, which depicts the cell type interactions of specific signaling pathways (Figure 7H–J), we found that in the BMF group, platelets release PF4, which acts specifically on the CXCR3 receptor of $CD4^+$/$CD8^+$ T cells.

3.8 | Gene Level and Related Protein Expression

Following the Multi-Omics Factor Analysis (MOFA) analysis, we noted that numerous genes pertinent to macrophage function, hematopoietic stem cell preservation, and T cell activation (including Adgre1, Tfrc, Kit, Il2ra, and Il12rb1) exhibited heightened correlation, while genes linked to cytotoxicity and

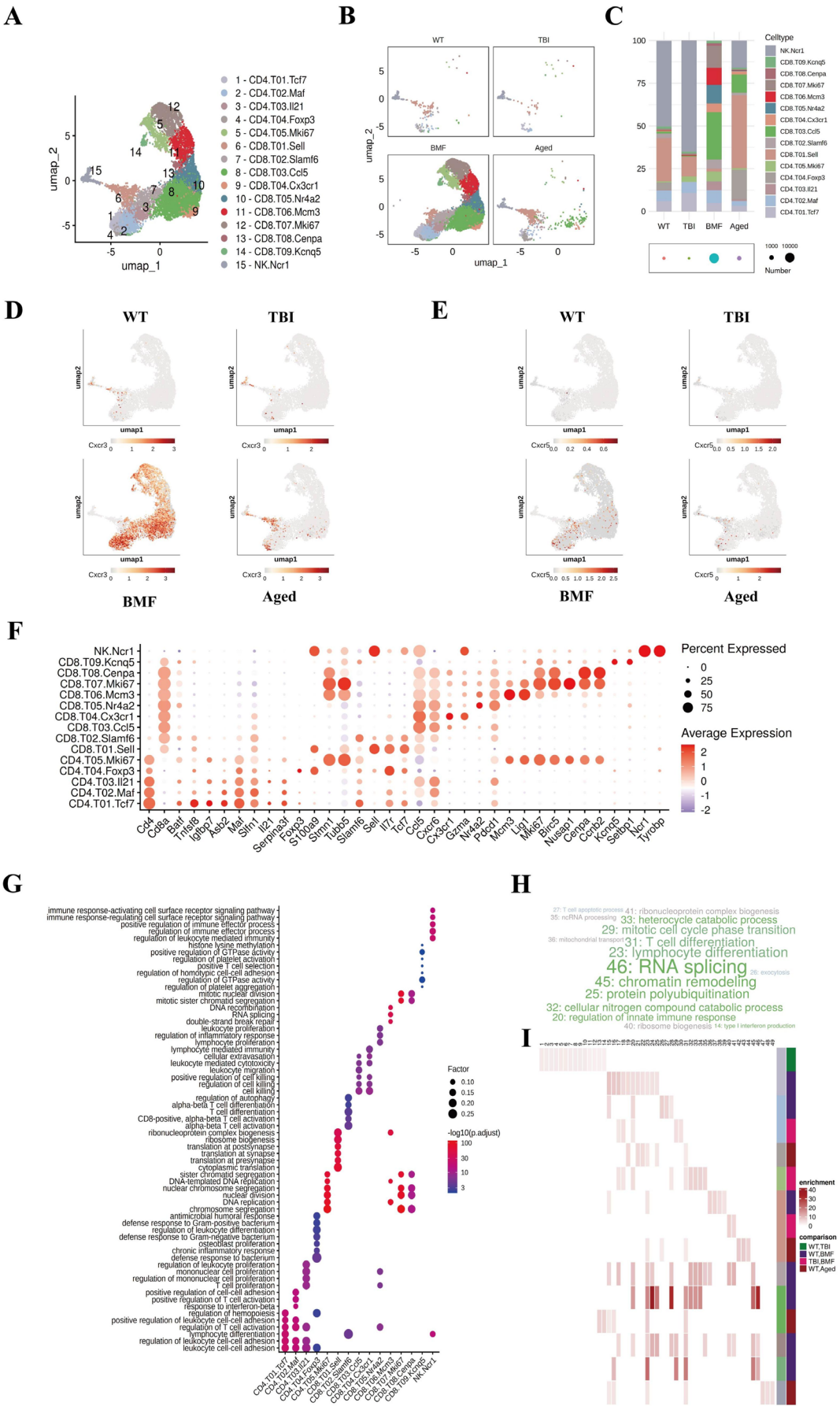

FIGURE 3 | Legend on next page.

FIGURE 3 | Immune Imbalance of $CD8^+$ T Cells/$CD4^+$ T Cells in BMF, with Heightened Expression of T Cell Membrane Receptor CXCR3. (A) UMAP plot showing 15 subtypes of TNK. (B) UMAP plot showing different subtypes of T/NK in different groups. (C) Bar chart showing the proportion of cells with specified T/NK subtypes in different groups. (D) UMAP dimensionality reduction displaying the expression of CXCR3 gene in four different TNK subtypes. (E) UMAP dimensionality reduction displaying the expression of CXCR5 gene in four different T/NK subtypes. (F) Bubble heatmap showing marker genes of different T/NK subtypes. The size of the dot represents the proportion of T/NK subtypes expressed, colored according to z-score. (G) Bubble heatmap showing signaling pathways of different T/NK subtypes. The size of the dot represents the proportion of CD4 T/NK subtypes expressed, colored according to *p*_val_adj. (H) Word cloud diagram showing enriched biological processes in samples/groups. The font size represents the enrichment frequency. (I) Heatmap showing the enrichment level of differentially expressed genes (DEGs) in different T/NK subtypes in different samples/groups. These numbers represent the enrichment scores.

immune regulation (such as Cd8a, Cxcr2, Pdcd1, and Ptprc) demonstrated diminished correlation (Figure S1A,B). We discovered that the Cd4 gene showed relatively high transcript levels in CD4+ T cells, macrophages, and platelets, but the corresponding CD4 antibody signal was decreased when we further compared transcript signals with antibody-derived protein signals (Figure S1C). While the antibody signal for the IFNGR1 gene was higher in B cell precursors but lower in T cells and neutrophils, the gene was also widely expressed across a variety of cell types.

3.9 | Enhanced Mitochondrial Energy Metabolism Signaling Pathway/TFAM Expression in BMF T Cells

By analyzing the expression intensity of various signaling pathways in different cells, we observed that within the T/NK cell subpopulation (Figure S2A,B), TFAM exhibits high expression levels in $CD8^+$ stress T cells of the BMF group, while this type of T cell in the TBI group shows almost no expression of TFAM.

Within macrophages (Figure S2A,C), TFAM (mitochondrial transcription factor A) is highly expressed in M1 cells in the Aged group and in Mph05 cells in the BMF group. Additionally, TLR expression is heightened in M1 cells in the Aged group, while the expression of PhosphoAkt, JAK, and ROS signaling pathways is higher in M2 cells in the WT group compared to the BMF group. Neutrophils were significantly reduced in the BMF group, and the remaining naive cells exhibited high expression of AMPK and NF-κB signaling pathways (Figure S2A,D).

The NOTCH, IFNG, NF-κB, and P53 signaling pathways are highly expressed in naive B cells in the BMF group. Interestingly, AMPK is virtually not expressed in naive B cells of the BMF group (Figure S2A,E).

3.10 | Characteristics of HSPCs, Neutrophils, and B/Plasma Cells in BMF

We continued analyzing the immune characteristics of various progenitor cells, using UMAP dimensionality reduction to display 17 progenitor cell types (Figure S3A). We also presented their distribution and proportions among the four groups (Figure S3B,C). In BMF, the total number of hematopoietic stem/progenitor cells significantly decreased, with megakaryocyte/platelets accounting for nearly 25% and neutrophil precursors accounting for 50% among the remaining progenitor cell types. Compared to the control group, B-lineage cells completely disappeared. Through analysis of the differential genes and functional enrichment of each progenitor cell (Figure S3D,E), we discovered heterogeneity changes among them. Furthermore, we examined the upregulation of functional expression in each lineage progenitor cell among the groups (Figure S3F,G). Although the proportion of B-lineage progenitor cells significantly decreased in the Aged group, their expression related to immune response and viral defense was upregulated. Additionally, the BMF group also upregulated the bacterial response process compared to the TBI group.

To further analyze the relationship between neutrophils and different samples/groups, we visualized the dimensionality reduction and clustering results using UMAP plots, presenting six types of neutrophils (Figure S4A). We analyzed the specific changes of these six types of neutrophils in AA and compared their distribution and proportion among the four groups (Figure S4B,C). In the BMF group, the total number of neutrophils was significantly decreased. Among the few remaining cells, Neu02 and Neu03 accounted for nearly 100%. Using enrichment analysis to determine the functional roles and related pathways of each neutrophil DEG (Figure S4D–H). Compared to the WT and TBI groups, the BMF group showed upregulated expression of genes related to apoptosis, proliferation, signaling, and immune-inflammatory responses in naive neutrophils.

We further analyzed the subt of B-cell genes and their relative distribution among the four groups (Figure S5A–C). In the WT and Aged groups, there was no significant decrease in the total number of B cells, though the proportion of mature B cells in Aged was slightly lower than that in WT. In the BMF group, the number of three types of B cells decreased significantly, with plasma cells accounting for the highest proportion among the remaining cells. To evaluate the unique biological characteristics of B-cell subsets, we utilized the "GSEA" function to perform pathway enrichment analysis on differentially expressed genes (DEGs) from various cell types and diseases (Figure S5D–F). In the inter-group comparison (Figure S5G), for the BMF group compared to the TBI group, plasma cells showed upregulated expression of the apoptosis signaling pathway, maintenance of cell number homeostasis, and post-translational modification of proteins.

3.11 | Long Non-Coding RNA (lncRNA)

We also investigated the expression levels of several long non-coding RNAs (lncRNAs) in various cells and groups (Figure S6).

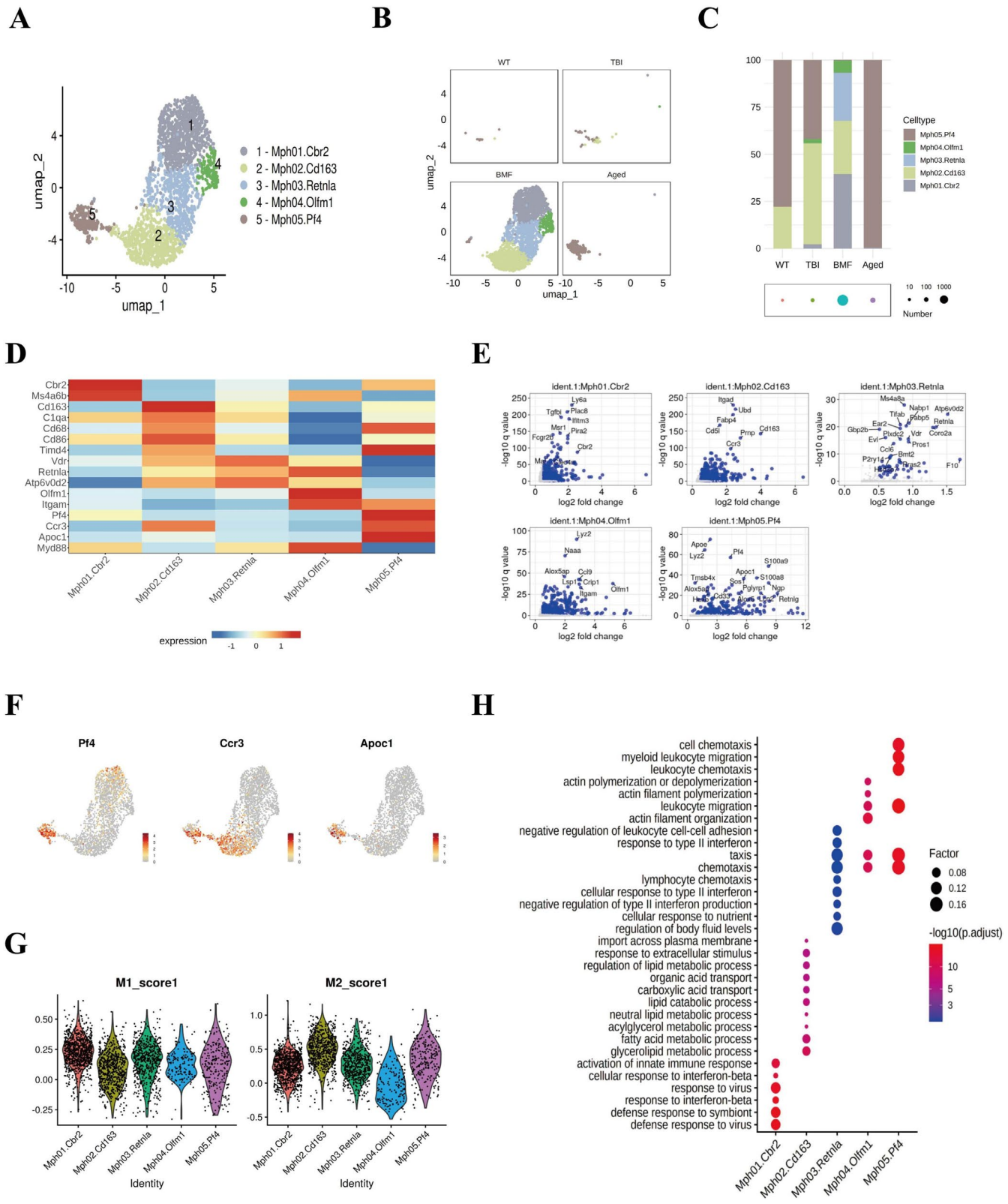

FIGURE 4 | Phenotype imbalance of M1/M2 in BMF, Leading to "Excessive Immune Response"; During Aging, new-type macrophage become enriched. (A) UMAP plot showing five macrophage subtypes. (B) UMAP plot showing different macrophage subtypes in four groups. (C) Bar chart showing the cell proportion of specified macrophage subtypes in four groups. (D) Heatmap showing differential gene enrichment in different macrophages, with colors representing expression levels. (E) Volcano plot showing marker genes in different macrophage subtypes. (F) UMAP plot showing marker genes (Pf4, Ccr3, Apoc1) in Mph05. (G) Violin plot showing M1/M2 scores of different macrophage subtypes. (H) Bubble heatmap showing signaling pathways between different macrophage subtypes. The size of the dots represents the proportion of expressing macrophage subtypes, colored according to *p*_val_adj.

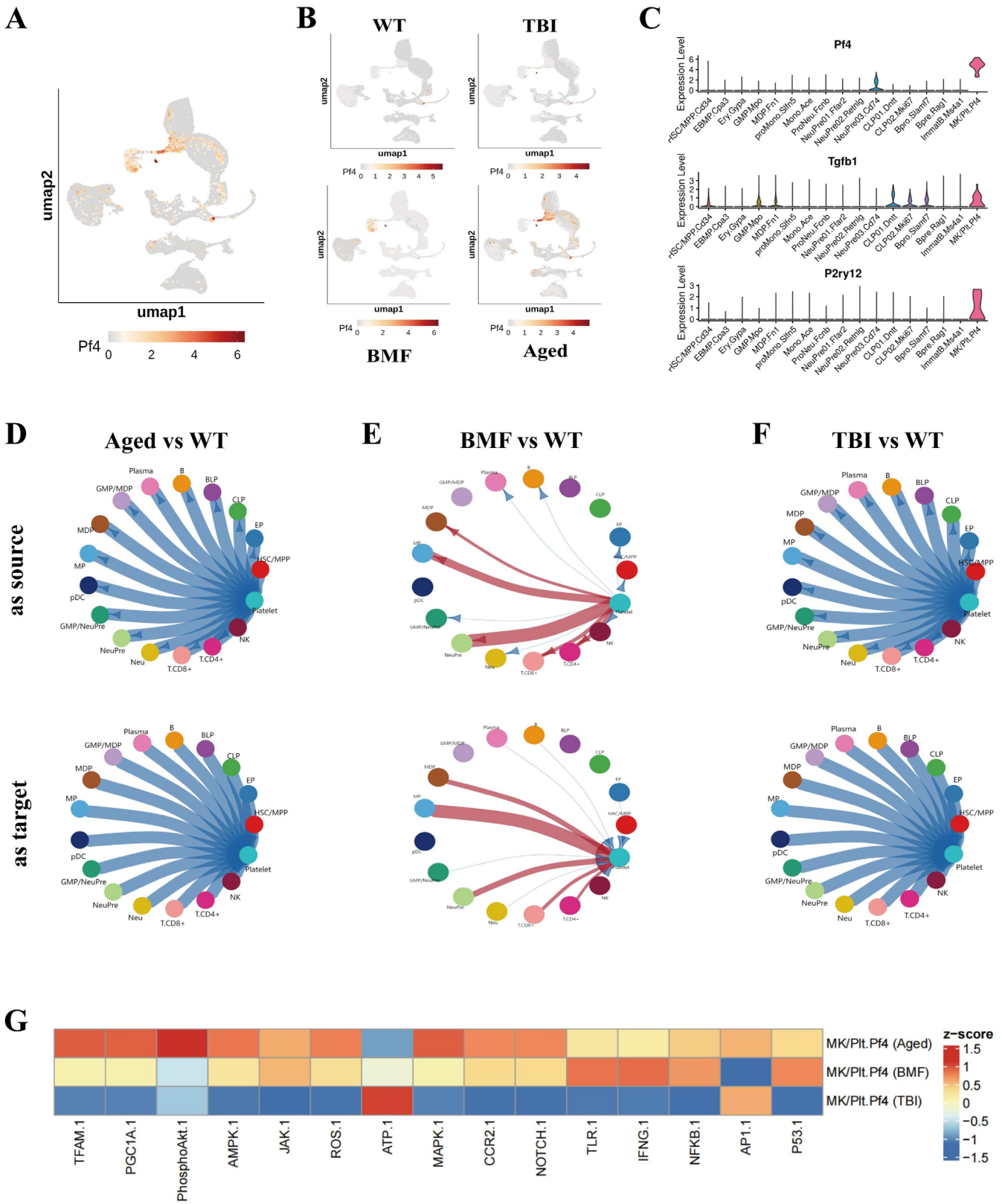

FIGURE 5 | Enhanced Crosstalk Between Platelets, T Cells, and Macrophages in BMF. (A) UMAP plot illustrating the enrichment of the Pf4 gene in various cell types. (B) Reduced-dimensionality UMAP plot demonstrating the enrichment of the Pf4 gene in four groups of cells. (C) Genes specifically expressed in platelets. (D) Network diagram of PLTs as sources and targets with other cell types in Aged and WT. (E) Network diagram of PLTs as sources and targets with other cell types in BMF and WT. (F) Network diagram of PLTs as sources and targets with other cell types in TBI and WT. (G) Heatmap showing the enrichment of various signaling pathways in platelets. Colored based on z-score.

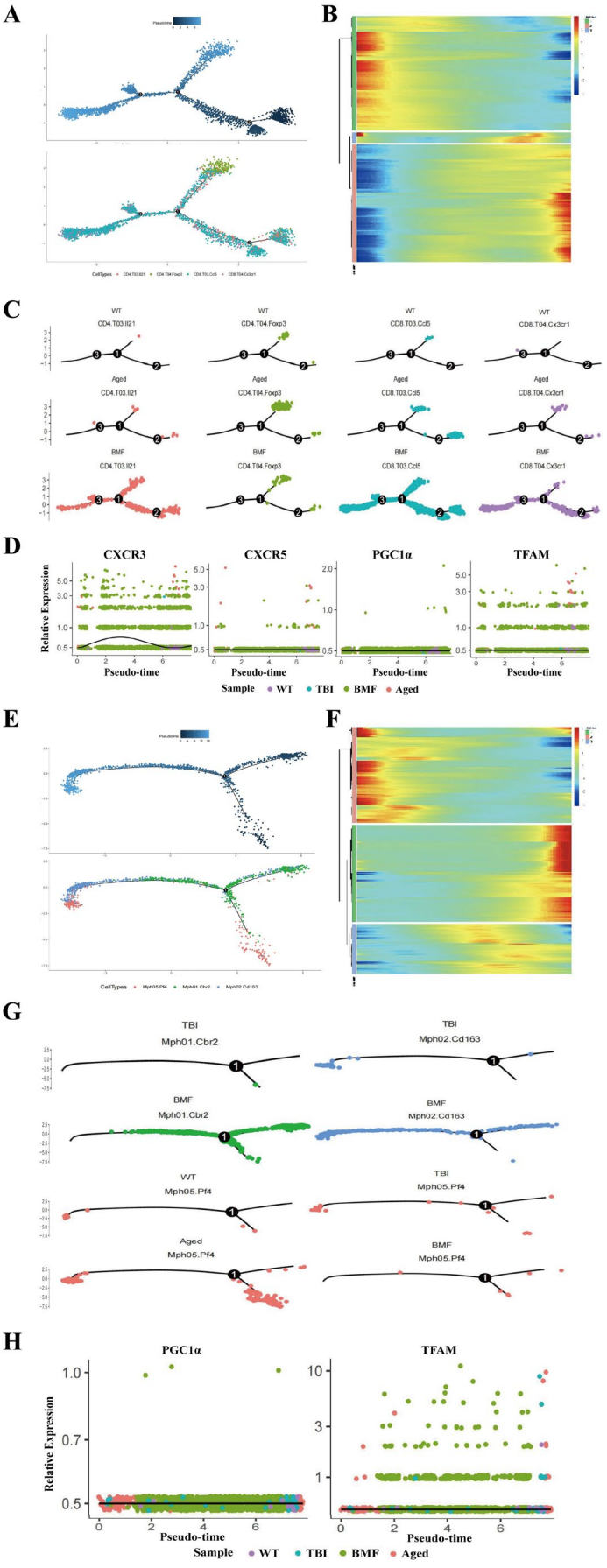

FIGURE 6 | Legend on next page.

FIGURE 6 | Pseudotime analysis of T cells and macrophages. (A) Pseudotime analysis was performed on four types of T cells, with the temporal order being ②→①→③. (B) Expression changes of differentially expressed genes over time. Different colors of clusters represent different gene sets, and the color intensity indicates gene expression levels, with red indicating higher expression. (C) Distribution trajectories of the four types of T cells are shown separately. (D) Expression changes of genes and proteins over time in the four types of T cells are shown separately. (E) Pseudotime analysis was performed on three types of macrophages, with the temporal order being from right to left. (F) Expression changes of differentially expressed genes over time. Different colors of clusters represent different gene sets, and the color intensity indicates gene expression levels, with red indicating higher expression. (G) Distribution trajectories of the three types of macrophages are shown separately. (H) Display the expression of two mitochondrial pathway proteins over time in three types of macrophages.

In the BMF group, the Hotairm1 gene had higher expression levels in MPs, and the Dleu2 gene had the highest expression in NK cells. In the TBI group, the H19 gene was highly expressed in GMPs and NeuPre, the Hotairm1 gene had higher expression levels in MPs and MDPs, and the Ttc39aos1 gene was highly expressed in GMPs and MDPs (The abbreviations in this paper are listed in Table S1).

4 | Discussion

AA is a classic symptom of BMF syndrome [18]. Current pathogenesis research primarily focuses on $CD8^+$ T cells, specifically CTLs. However, the role of platelets, $CD4^+$ T cells, macrophages, and other immune cells in BMF remains unclear [19, 20]. Our research team previously identified the mitochondrial-mediated Akt-PGC1α-TFAM pathway, platelet release PF4, and the regulation of T cell immune responses [12, 21]. Due to the reduction in BMF and whole blood cells in AA patients, it is challenging to collect sufficient cell numbers for research. We successfully constructed a BMF mouse model closely resembling AA patients' pathophysiology and, for the first time, used single-cell transcriptomics to comprehensively analyze the single-cell atlas of immune responses in the BMF mouse model.

4.1 | T Cells in BMF and Membrane Receptors CXCR3/CXCR5

Previous studies indicate that in the bone marrow microenvironment of AA patients, there is excessive accumulation of T cells accompanied by a significant reduction in the proportion of Tregs [22, 23]. Tregs, marked by high Foxp3 expression, suppress immunity and their deficiency can cause autoimmune diseases [24]. In the BMF group, platelet-released PF4 can bind to the membrane receptor CXCR3, stimulating T cells' immune responses and enhancing the Treg phenotype [25]. In the BMF group, Tfh cells rose, fueling inflammation, $CD8^+$ T cell activation, and IFN-γ secretion [26]. Similarly, TEM cells, providing immediate immune protection in local tissues, are more abundant than in the TBI group. In SAA patients, their memory T cells are highly activated, leading to an attack on bone marrow hematopoietic cells [27]. This promotes the development of an inflammatory environment and exacerbates the damage to the bone marrow microenvironment [28].

Consistent with prior research, we noted a significant rise in $CD8^+$ T cells, which may crucially mediate immunity in AA [29]. Among the increased $CD8^+$ T cell subsets, effector T cells were more abundant, while naive T cells were significantly reduced compared to other groups. After recognizing antigens, naive $CD8^+$ T cells differentiate into effector T cells or CTLs. Activated effector cells can damage target cells upon subsequent recognition of antigens [30, 31].

CXCR3 is an inflammatory chemokine receptor mainly on CTLs [32]. In our previous research, we discovered that PLT regulates TCM/TEM cells by secreting PF4, which attaches to CXCR3 and triggers the downstream mitochondrial metabolic signaling pathway of Akt-PGC1α-TFAM [12, 33]. Additionally, we found that CXCR5 expression was significantly elevated in $CD4^+$/$CD8^+$TEM cells, while CXCR3 expression was significantly upregulated in T-cell subsets except $CD4^+$Treg cells, and $CD8^+$naïve T cells in the current single-cell sequencing investigation. PF4 generated from megakaryocytes is abnormally high in the bone marrow fibrosis (MF) model, and it modulates T cell subsets, such as $CXCR5^+$ T cells, to accelerate the advancement of bone marrow fibrosis [34]. Myeloproliferative neoplasms (MPNs) have a molecular foundation because PF4 controls HSC homeostasis through CXCR3/CXCR5 [35]. In particular, PF4 activates the mitochondrial metabolic pathway (Akt-PGC1α-TFAM) and mediates immunological dysregulation in AA by binding to CXCR3 and CXCR5 on the surface of $CD4^+$ and $CD8^+$ T cells [36]. Collectively, we speculate that in our BMF model, the binding of PF4 to CXCR3/CXCR5 serves as a critical regulatory pathway that modulates T cell dysfunction and drives the pathological progression of bone marrow failure. NK cells were significantly decreased or absent in BMF, potentially reducing regulation of auto reactive [37, 38].

4.2 | Macrophage Differentiation/Change in BMF and Aging

Previous studies showed that M2 macrophages promote MK and platelet production, while M1 macrophages may inhibit these processes [39]. Additionally, in the aging group, we identified Mph05 macrophage expressing high Cd68, Pf4, S100a8/a9, Apoc1, and CCR3, but low expression of Cd163 and C1qa.

Further investigation revealed that Mph05 macrophages differ from M4 macrophages, which are induced by PF4 and co-express CD68, S100A8, and MMP7. Notably, the combination of MMP7 and S100A8 serves as a specific marker for identifying M4 macrophages [40, 41].

This profile does not align clearly with classical M1 or M2 polarization, and M4 macrophages are distinct from the Mph05 macrophages identified in our study [42].

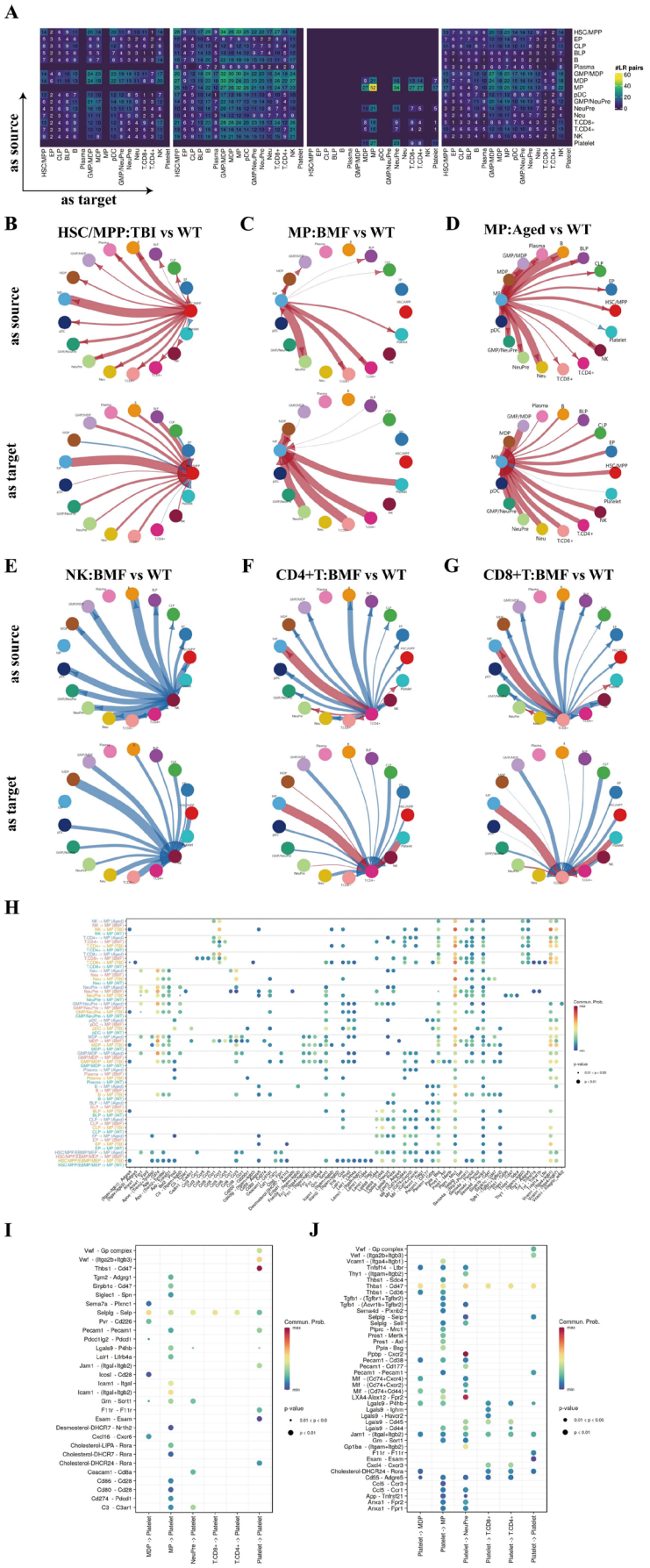

FIGURE 7 | Legend on next page.

FIGURE 7 | During BMF, platelets release PF4 and interact with T cells and macrophages. (A) Heatmap showing the interaction strength between cell types in different samples/groups. The numbers indicate the number of LR pairs. (B) Network diagram of HSCs/MPPs in TBI and WT as source and target cells, respectively, interacting with other cell types. (C) Network diagram of MPs in BMF and WT as source and target cells, respectively, interacting with other cell types. (D) Network diagram of platelets in BMF versus WT as source and target cells, respectively, interacting with other cell types. (E) Network diagram of NK cells in BMF and WT as source and target cells, respectively, interacting with other cell types. (F) Network diagram of $CD4^+$ T cells in BMF and WT as source and target cells, respectively, interacting with other cell types. (G) Network diagram of $CD8^+$ T cells in BMF and WT as source and target cells, respectively, interacting with other cell types. (H) Bubble heatmap showing the communication probability of L-R interactions between different cell types in different sample.

4.3 | PF4 in Macrophage Differentiation and Chemotaxis in BMF and Aging

PF4 in the bone marrow is primarily produced by MKs and increasing the number of quiescent HSCs [35, 43, 44]. Previous studies in BMF models showed that MKs can activate Th and $CD8^+$ T cells, contributing to HSC cytotoxicity [45, 46]. In addition, tumor-associated macrophages (TAMs) have been reported to produce PF4, which may lead Tregs to Th1-like phenotype (Th1-Treg cells), and hypoxic microenvironments can enhance glycolysis and potentially PF4 expression [47]. Thus, the S100A8/A9-driven inflammatory axis may represent a critical checkpoint in the transition from BMF to myeloid malignancy.

In our study, we observed a significant upregulation of S100A8/A9 within the Mph05 subset, aligning with its role as a pivotal biomarker for assessing disease activity and therapeutic efficacy in BMF syndromes [48]. While systemic S100A8/A9 levels typically increase with aging across various tissues, their aberrant expression in the bone marrow niche is specifically linked to immune-mediated marrow destruction and treatment resistance in SAA [49–51]. Mechanistically, while S100A9 is essential for M1-type macrophage polarization, its sustained overexpression—as seen in our Mph05 population—likely triggers the TLR4/NF-κB inflammatory cascade, thereby impairing myeloid differentiation and fostering a pro-leukemic microenvironment conducive to MDS progression [52, 53].

Apoc1 is also highly expressed in Mph05. Apoc1 promotes polarization toward the M2 phenotype [21]. Based on the marker genes, Mph05 appears to be involved in chemotaxis and increases with age. However, whether these cells directly contribute to pathological BMF or preferentially phagocytose senescent cells remains to be experimentally determined.

4.4 | Platelets in Aging and BMF: Immune Regulatory Roles

In the Aged group, the gene PF4 is highly expressed specifically in platelets. Previous studies suggested that PF4 supports HSC function via CXCR3 signaling [43], and our data show increased PF4 expression in aging bone marrow, implying a potential role in maintaining HSC function. Platelets-drived PF4 can interact with CXCR3 on $CD4^+$/$CD8^+$ T cells, potentially enhancing immune responses and modulating Th1-Treg plasticity [47].

In the BMF group, PF4 may also act on macrophages, promoting polarization of the Mph05 subset and enhancing phagocytic activity, consistent with reports that PF4 boosts macrophage phagocytosis without increasing cell number [54]. In aging bone marrow, Mph05 is abundant, which may reflect homeostatic phagocytosis of senescent macrophages rather than pathological activity [11].

We observed that platelets provide VCAM1, which can engage macrophage ITGA4 and may promote M1 polarization, in line with previous studies linking VCAM1-ITGA4 to pro-inflammatory signaling [55, 56]. Furthermore, platelets from the BMF group displayed relatively low levels of PGC1α, AMPK, and CCR2 pathway proteins, consistent with the importance of mitochondrial function in platelet activation and apoptosis under the hypoxic bone marrow environment [57, 58].

4.5 | Mitochondrial Energy Metabolism Pathway in BMF

AMPK and PGC1α are regulators of energy homeostasis and mitochondrial biogenesis [59, 60]. AMPK phosphorylates PGC-1α, increasing mitochondrial gene expression [60]. In our study, platelets from the BMF group exhibited increased ROS levels compared to the TBI group, consistent with oxidative stress potentially impairing HSC self-renewal [32, 61].

We observed strong TFAM expression in $CD8^+$T09Kcn95 cells ($CD8^+$stress T cells) in the BMF group, whereas TFAM was nearly absent in the TBI group. TFAM is essential for mtDNA replication and mitochondrial biogenesis [62–64], and its upregulation likely reflects increased energy demands in stressed T cells. Similarly, TFAM was moderately expressed in new-type macrophages in the Aged group but strongly expressed in the BMF group, suggesting robust mitochondrial metabolism in these cells.

Although M1-type macrophages in the Aged group and Mph05 in the BMF group are relatively low in proportion, high TFAM and S100A9 expression indicate metabolic activity. These observations suggest that new-type macrophages may contribute to HSC pyroptosis in the bone marrow, whereas T cells are primarily involved in HSC apoptosis [65, 66].

4.6 | Expression of TFAM and TLR in M1 Macrophages and Their Role in BMF

Our results show increased expression of TFAM and TLR in M1 macrophages from the Aged group. Toll-like receptors (TLRs) can promote M1 macrophage polarization [67]. Peripheral blood-derived macrophages from SAA patients expressed elevated

TLR4 expression, contributing to inflammatory cascades and HSC/hematopoietic progenitor cell damage [68]. We discovered that bone marrow M1 macrophages from old mice had higher TLR expression, indicating that SAA and aging can be related to a vicious loop of myeloid inflammation driven by TLR4.

In the BMF group, ATP pathway proteins were expressed at lower levels compared to the TBI group. Although platelet numbers are reduced in BMF, their immune functions appear preserved. However, platelets may exhibit impaired aggregation and adhesion under pathological conditions [69].

4.7 | CCI in BMF

In our study, HSPCs showed strong interactions with macrophages, indicating a central role for macrophages in intercellular communication. In the BMF group, platelets released PF4, which may bind CXCR3 on $CD4^+$ and $CD8^+$ T cells and activate downstream mitochondrial energy metabolism pathways [33]. This finding establishes the existence of a platelet-PF4-$CD4^+$ T cell-$CD8^+$ T cell-CXCR3 relationship in BMF. The secretion of PF4 by platelets may cause T cell polarization through binding to CXCR3 on T cells, thereby contributing to BMF. Shaorong Deng's team suggested that exogenous and overexpressed PF4 can directly stimulate $CD8^+$ T cells through CXCR3 to activate caspase-3, leading to apoptosis and inhibiting anti-tumor immunity [70].

4.8 | Pseudotime Analysis of T Cells and Macrophages

Tregs were mainly distributed in the late phase of the aged group's time trajectory, indicating their primary role in suppressing autoreactive T cell activation in aged bone marrow [24]. Tfh cells, which exhibit plasticity in physiological environments to tailor immune responses to various pathogens or antigens, may become pathogenic in autoimmune diseases due to dysregulated cytokine environments, accelerating bone marrow failure [25]. CXCR3 expression surged over time in the BMF group, which would make it possible for platelet-derived PF4 to interact with CXCR3 and trigger downstream mitochondrial signaling, which could lead to T cell imbalance and bone marrow failure. Throughout the BMF process, both M1 and M2 macrophages were active. M1 macrophages secreted TNF-α and IFN-γ, which are known to be negative regulators of hematopoiesis [47, 71]. In contrast, the new-type macrophages primarily function in aged bone marrow without causing pathological bone marrow failure.

4.9 | Single-Cell Atlas Characteristics of HSPCs, Neutrophils, and B/Plasma Cells in BMF

We observed a significant reduction in total HSPCs in the BMF group. Among the remaining progenitor cells, megakaryocytes/platelets accounted for nearly 25%, while neutrophil precursors accounted for over 50%, suggesting that neutrophil differentiation may be important for maintaining hematopoietic balance [72]. In the Aged group, the proportion of B-lineage progenitor cells was significantly decreased. In elderly mice, the number of common lymphoid progenitors (CLP), pre-pro-B cells, and pro-B cells decreases [73]. Within the BMF group, all three B cell types declined, with plasma cells comprising the largest proportion of remaining B cells. Plasma cells also showed upregulated protein post-translational modification, which may reflect increased autoantibody production. Abnormal autoantigen levels, including anti-Moesin antibodies, have been reported in AA and can potentially contribute to hematopoietic suppression via myelosuppressive cytokines [74].

4.10 | LncRNA in BMF

In the BMF group, the myeloid-specific lncRNA Hotairm1 was highly expressed in macrophages, while in aging bone marrow, Hotairm1 showed the highest expression in platelets, suggesting a role in maintaining platelet numbers via interactions with the p53 signaling pathway [75, 76]. NK cells were significantly reduced or absent in the BMF group, with Dleu2 expression highest in remaining NK cells, which may contribute to NK cell depletion [77].

Consistent with these findings, platelets release PF4 to engage T cell receptors CXCR3 and CXCR5, potentially activating mitochondrial energy metabolism pathways. During this process, Treg cells decreased, weakening immunosuppressive effects, while $CD8^+$ stress T cells exhibited increased energy metabolism, supporting cytotoxic activity. Pro-inflammatory M1 macrophages were elevated, while anti-inflammatory M2 macrophages were reduced. In contrast, new-type macrophages and $CD8^+$ naive T cells, although associated with aging, did not appear to directly drive pathological BMF.

These observations indicate that platelet-mediated crosstalk with T cells and macrophages, along with lnc RNA regulations, may contribute to immune imbalance and BMF. Targeting immune cell plasticity and platelet-mediated signaling may represent a potential therapeutic strategy for restoring bone marrow homeostasis in AA.

5 | Limitations of the Study

This study has some limitations. First, despite the fact that the BMF mouse model replicates the clinical features of AA, there are species differences between humans and animals with regard to immunological networks and the hematopoietic milieu. Second, statistical power might be impacted by the small sample size. Third, to further validate our findings, we need to run cross-comparative studies with single-cell sequencing data from AA patients and basic assays (such as flow cytometry, immunofluorescence, and Western blot). Furthermore, the generalizability and intervention effects of the possible therapeutic approaches have not been confirmed in clinical samples.

Author Contributions

Shuai Tan: conceptualization (equal), investigation (equal), methodology (equal), writing – original draft (equal), writing – review and editing

(equal). **Fang Fang:** conceptualization (equal), investigation (equal), methodology (equal), writing – original draft (equal). **Jing Sun:** conceptualization (equal), investigation (equal), methodology (equal), writing – original draft (equal). **Yumeng Li:** data curation (equal), writing – original draft (equal), writing – review and editing (equal). **Yaochi Chen:** data curation (equal), writing – original draft (equal), writing – review and editing (equal). **Wanling Sun:** funding acquisition (equal), investigation (equal), methodology (equal), supervision (equal).

Acknowledgments

The study was supported by grants from the Natural Science Foundation of Beijing Municipality (project no Z200022); the National Natural Science Foundation of China (NSFC) (project no 82300161); Beijing High Innovation Program·Spring Bud Project (project no 2-1-008-0262); Xuanwu Hospital Talent Convergence Program (project no HZ2025ZCYX003); Beijing Future Talent Training Program in Medical-Engineering Field (project no MBRC0012025063); Beijing High-level Overseas Returnee Talent Funding Project (project no 2-2-008-0243), Capital Medical University Science and Innovation Elite Plan Project (project no 2024KCJY0405); the "National Natural Science Foundation of Youth Cultivation Project" of "Xuanwu Hospital, Capital Medical University, Beijing, China" (project no QNPY2022014); the "Person of Outstanding Ability Training Program" of "Xuanwu Hospital, Capital Medical University, Beijing, China" (project no YC20220127). All authors provided critical feedback during manuscript preparation and approved the final version for publication.

Funding

The study was supported by grants from the Natural Science Foundation of Beijing Municipality (project no Z200022); the National Natural Science Foundation of China (NSFC) (project no 82300161); Beijing High Innovation Program Spring Bud Project (project no 2-1-008-0262); Xuanwu Hospital Talent Convergence Program (project no HZ2025ZCYX003); Beijing Future Talent Training Program in Medical-Engineering Field (project no MBRC0012025063); Beijing High-level Overseas Returnee Talent Funding Project (project no 2-2-008-0243), Capital Medical University Science and Innovation Elite Plan Project (project no 2024KCJY0405), the "National Natural Science Foundation of Youth Cultivation Project" of "Xuanwu Hospital, Capital Medical University, Beijing, China" (project no QNPY2022014), the "Person of Outstanding Ability Training Program" of "Xuanwu Hospital, Capital Medical University, Beijing, China" (project no YC20220127). All authors provided critical feedback during manuscript preparation and approved the final version for publication.

Conflicts of Interest

The authors declare no conflicts of interest.

Data Availability Statement

All raw data from this study are available in the GEO database under accession number GSE305447. All data reported in this paper will be shared by the lead contact upon request. Any additional information required to reanalyze the data reported in this paper is available from the lead contact upon request.

References

1. C. A. Sieff, "Introduction to Acquired and Inherited Bone Marrow Failure," *Hematology/Oncology Clinics of North America* 32, no. 4 (2018): 569–580.

2. R. P. Gale, W. Hinterberger, N. S. Young, et al., "What Causes Aplastic Anaemia?," *Leukemia* 37, no. 6 (2023): 1191–1193.

3. V. Giudice and C. Selleri, "Aplastic Anemia: Pathophysiology," *Seminars in Hematology* 59, no. 1 (2022): 13–20.

4. J. Chen, M. J. Desierto, X. Feng, et al., "Immune-Mediated Bone Marrow Failure in C57BL/6 Mice," *Experimental Hematology* 43, no. 4 (2015): 256–267.

5. Z. Wu and N. S. Young, "Single-Cell Genomics in Acquired Bone Marrow Failure Syndromes," *Blood* 142, no. 14 (2023): 1193–1207.

6. C. Zhu, Y. Lian, C. Wang, et al., "Single-Cell Transcriptomics Dissects Hematopoietic Cell Destruction and T-Cell Engagement in Aplastic Anemia," *Blood* 138, no. 1 (2021): 23–33.

7. L. T. W. Vissers, M. M. van Ostaijen-Ten Dam, J. E. Melsen, et al., "Potential Role of B- and NK-Cells in the Pathogenesis of Pediatric Aplastic Anemia Through Deep Phenotyping," *Frontiers in Immunology* 15 (2024): 1328175.

8. Y. Chen, L. Luo, Y. Zheng, et al., "Association of Platelet Desialylation and Circulating Follicular Helper T Cells in Patients With Thrombocytopenia," *Frontiers in Immunology* 13 (2022): 810620.

9. N. Sun, M. Zhang, J. Kong, et al., "Dysregulated T-Cell Homeostasis and Decreased CD30(+) Treg Proliferating in Aplastic Anemia," *Heliyon* 10, no. 15 (2024): e35775.

10. N. Li, "CD4+ T Cells in Atherosclerosis: Regulation by Platelets," *Thrombosis and Haemostasis* 109, no. 6 (2013): 980–990.

11. N. Gerdes, L. Zhu, M. Ersoy, et al., "Platelets Regulate CD4(+) T-Cell Differentiation via Multiple Chemokines in Humans," *Thrombosis and Haemostasis* 106, no. 2 (2011): 353–362.

12. S. Tan, S. Li, Y. Min, et al., "Platelet Factor 4 Enhances CD4(+) T Effector Memory Cell Responses via Akt-PGC1alpha-TFAM Signaling-Mediated Mitochondrial Biogenesis," *Journal of Thrombosis and Haemostasis* 18, no. 10 (2020): 2685–2700.

13. D. Osorio and J. J. Cai, "Systematic Determination of the Mitochondrial Proportion in Human and Mice Tissues for Single-Cell RNA-Sequencing Data Quality Control," *Bioinformatics* 37, no. 7 (2021): 963–967.

14. A. McCabe, J. N. P. Smith, A. Costello, et al., "Hematopoietic Stem Cell Loss and Hematopoietic Failure in Severe Aplastic Anemia Is Driven by Macrophages and Aberrant Podoplanin Expression," *Haematologica* 103, no. 9 (2018): 1451–1461.

15. R. Ni, L. Fan, L. Zhang, et al., "A Mouse Model of Irradiation and Spleen-Thymus Lymphocyte Infusion Induced Aplastic Anemia," *Hematology* 27, no. 1 (2022): 932–945.

16. T. Stuart, A. Butler, P. Hoffman, et al., "Comprehensive Integration of Single-Cell Data," *Cell* 177, no. 7 (2019): 1888–1902.

17. S. Jin, C. F. Guerrero-Juarez, L. Zhang, et al., "Inference and Analysis of Cell-Cell Communication Using CellChat," *Nature Communications* 12, no. 1 (2021): 1088.

18. A. E. DeZern and J. E. Churpek, "Approach to the Diagnosis of Aplastic Anemia," *Blood Advances* 5, no. 12 (2021): 2660–2671.

19. H. Wang, Y. Chen, H. Deng, et al., "Comprehensive Mapping of Immune Perturbations Associated With Aplastic Anemia," *Cell Biology and Toxicology* 40, no. 1 (2024): 75.

20. N. S. Young, "Aplastic Anemia," *New England Journal of Medicine* 379, no. 17 (2018): 1643–1656.

21. L. Ren, J. Yi, Y. Yang, et al., "Systematic Pan-Cancer Analysis Identifies APOC1 as an Immunological Biomarker Which Regulates Macrophage Polarization and Promotes Tumor Metastasis," *Pharmacological Research* 183 (2022): 106376.

22. P. Scala, V. Giudice, D. Morini, A. M. Della Corte, C. Selleri, and B. Serio, "Circulating T Regulatory Cells Are Persistently Reduced in Non-Severe Acquired Aplastic Anemia," *Current Medical Science* 45 (2025): 977–984.

23. R. Guo, J. Kong, P. Tang, et al., "Unbiased Single-Cell Sequencing of Hematopoietic and Immune Cells From Aplastic Anemia Reveals

the Contributors of Hematopoiesis Failure and Dysfunctional Immune Regulation," *Advanced Science (Weinheim, Germany)* 11, no. 10 (2024): e2304539.

24. D. Qin, Y. Zhang, P. Shu, Y. Lei, X. Li, and Y. Wang, "Targeting Tumor-Infiltrating Tregs for Improved Antitumor Responses," *Frontiers in Immunology* 15 (2024): 1325946.

25. N. J. M. Verstegen, T. Jorritsma, A. Ten Brinke, et al., "TCR-CD3 Signal Strength Regulates Plastic Coexpression of IL-4 and IFN-Gamma in Tfh-Like Cells," *Frontiers in Immunology* 15 (2024): 1481243.

26. K. Asosingh, A. Vasanji, A. Tipton, et al., "Eotaxin-Rich Proangiogenic Hematopoietic Progenitor Cells and CCR3+ Endothelium in the Atopic Asthmatic Response," *Journal of Immunology (Baltimore, Md.: 1950)* 196, no. 5 (2016): 2377–2387.

27. W. W. Li, R. N. Li, L. L. Zhang, et al., "Kinetics of Immune Activated T Cells in Aplastic Anemia Mouse Model," *Zhonghua Xue Ye Xue Za Zhi* 43, no. 7 (2022): 581–586.

28. T. Braun, G. Carvalho, C. Fabre, et al., "Targeting NF-kappaB in Hematologic Malignancies," *Cell Death and Differentiation* 13, no. 5 (2006): 748–758.

29. T. Chu, S. Hu, J. Qi, et al., "Bifunctional Effect of the Inflammatory Cytokine Tumor Necrosis Factor Alpha on Megakaryopoiesis and Platelet Production," *Journal of Thrombosis and Haemostasis* 20, no. 12 (2022): 2998–3010.

30. D. M. Gravano and K. K. Hoyer, "Promotion and Prevention of Autoimmune Disease by CD8+ T Cells," *Journal of Autoimmunity* 45 (2013): 68–79.

31. C. Liu, Y. Sun, and Z. Shao, "Current Concepts of the Pathogenesis of Aplastic Anemia," *Current Pharmaceutical Design* 25, no. 3 (2019): 236–241.

32. E. C. Cheung and K. H. Vousden, "The Role of ROS in Tumour Development and Progression," *Nature Reviews Cancer* 22, no. 5 (2022): 280–297.

33. S. Tan, J. Zhang, Y. Sun, et al., "Platelets Enhance CD4+ Central Memory T Cell Responses via Platelet Factor 4-Dependent Mitochondrial Biogenesis and Cell Proliferation," *Platelets* 33, no. 3 (2022): 360–370.

34. D. Capitanio, F. R. Calledda, V. Abbonante, et al., "Proteomic Screening Identifies PF4/Cxcl4 as a Critical Driver of Myelofibrosis," *Leukemia* 38, no. 9 (2024): 1971–1984.

35. I. Bruns, D. Lucas, S. Pinho, et al., "Megakaryocytes Regulate Hematopoietic Stem Cell Quiescence Through CXCL4 Secretion," *Nature Medicine* 20, no. 11 (2014): 1315–1320.

36. S. Tan, H. He, Y. Li, et al., "Platelets as a Potential New Immune Coordinator in T Cell-Mediated Aplastic Anemia," *Frontiers in Oncology* 15 (2025): 1568169.

37. C. M. Schurch, C. Caraccio, and M. A. Nolte, "Diversity, Localization, and (Patho)physiology of Mature Lymphocyte Populations in the Bone Marrow," *Blood* 137, no. 22 (2021): 3015–3026.

38. S. Lundgren, J. Huuhtanen, M. Keranen, et al., "Single-Cell Analysis of Aplastic Anemia Reveals a Convergence of NK and NK-Like CD8(+) T Cells With a Disease-Associated TCR Signature," *Science Translational Medicine* 17, no. 787 (2025): eadl6758.

39. H. Zhao, "From Traditional Chinese Medicine Formulations to Effective Anticancer Agents: Insights From Calculus Bovis," *World Journal of Gastroenterology* 30, no. 35 (2024): 4011–4013.

40. H. Jinnouchi, L. Guo, A. Sakamoto, et al., "Diversity of Macrophage Phenotypes and Responses in Atherosclerosis," *Cellular and Molecular Life Sciences* 77, no. 10 (2020): 1919–1932.

41. C. Erbel, M. Tyka, C. M. Helmes, et al., "CXCL4-Induced Plaque Macrophages Can Be Specifically Identified by Co-Expression of MMP7+S100A8+ In Vitro and In Vivo," *Innate Immunity* 21, no. 3 (2015): 255–265.

42. L. Zhang, Z. Li, K. M. Skrzypczynska, et al., "Single-Cell Analyses Inform Mechanisms of Myeloid-Targeted Therapies in Colon Cancer," *Cell* 181, no. 2 (2020): 442–459.

43. Z. Liu, L. Li, H. Zhang, et al., "Platelet Factor 4(PF4) and Its Multiple Roles in Diseases," *Blood Reviews* 64 (2024): 101155.

44. L. Lecomte-Raclet, M. Alemany, A. Sequira-Le Grand, et al., "New Insights Into the Negative Regulation of Hematopoiesis by Chemokine Platelet Factor 4 and Related Peptides," *Blood* 91, no. 8 (1998): 2772–2780.

45. A. Prabahran, L. Wu, A. L. Manley, et al., "Mature Megakaryocytes Acquire Immune Characteristics in a Mouse Model of Aplastic Anemia," *Blood Advances* 9, no. 13 (2025): 3315–3330.

46. F. Norozi, S. Shahrabi, S. Hajizamani, and N. Saki, "Regulatory Role of Megakaryocytes on Hematopoietic Stem Cells Quiescence by CXCL4/PF4 in Bone Marrow Niche," *Leukemia Research* 48 (2016): 107–112.

47. A. Kuratani, M. Okamoto, K. Kishida, et al., "Platelet Factor 4-Induced T(H)1-T(Reg) Polarization Suppresses Antitumor Immunity," *Science* 386, no. 6724 (2024): eadn8608.

48. S. Wang, R. Song, Z. Wang, Z. Jing, and J. Ma, "S100A8/A9 in Inflammation," *Frontiers in Immunology* 9 (2018): 1298.

49. W. R. Swindell, A. Johnston, X. Xing, et al., "Robust Shifts in S100a9 Expression With Aging: A Novel Mechanism for Chronic Inflammation," *Scientific Reports* 3 (2013): 1215.

50. S. A. Doodnauth, S. Grinstein, and M. E. Maxson, "Constitutive and Stimulated Macropinocytosis in Macrophages: Roles in Immunity and in the Pathogenesis of Atherosclerosis," *Philosophical Transactions of the Royal Society of London. Series B, Biological Sciences* 374, no. 1765 (2019): 20180147.

51. V. Giudice, Z. Wu, S. Kajigaya, et al., "Circulating S100A8 and S100A9 Protein Levels in Plasma of Patients With Acquired Aplastic Anemia and Myelodysplastic Syndromes," *Cytokine* 113 (2019): 462–465.

52. C. Gong, J. Ma, Y. Deng, et al., "S100A9(−/−) Alleviates LPS-Induced Acute Lung Injury by Regulating M1 Macrophage Polarization and Inhibiting Pyroptosis via the TLR4/MyD88/NFkappaB Signaling Axis," *Biomedicine & Pharmacotherapy* 172 (2024): 116233.

53. Y. Wang, C. Lin, C. Yao, et al., "High BM Plasma S100A8/A9 Is Associated With a Perturbed Microenvironmentand Poor Prognosis in Myelodysplastic Syndromes," *Blood Advances* 7, no. 11 (2023): 2528–2533.

54. O. Pervushina, B. Scheuerer, N. Reiling, et al., "Platelet Factor 4/CXCL4 Induces Phagocytosis and the Generation of Reactive Oxygen Metabolites in Mononuclear Phagocytes Independently of Gi Protein Activation or Intracellular Calcium Transients," *Journal of Immunology (Baltimore, Md.: 1950)* 173, no. 3 (2004): 2060–2067.

55. L. Wang, Y. Tang, J. Tang, et al., "Endothelial Cell-Derived Extracellular Vesicles Expressing Surface VCAM1 Promote Sepsis-Related Acute Lung Injury by Targeting and Reprogramming Monocytes," *Journal of Extracellular Vesicles* 13, no. 3 (2024): e12423.

56. C. K. Baldauf, C. Fahldieck, A. Angenstein, et al., "Activation of Integrin Signaling Up-Regulates Pro-Inflammatory Cytokines in JAK2-V617F Positive Hematopoietic Cells," *Cell Communication and Signaling: CCS* 23, no. 1 (2025): 368.

57. H. Li, C. Zhou, Y. Shen, M. Xu, D. Wu, and B. Ye, "Research Progress on the Hematopoietic Microenvironment in Aplastic Anemia," *European Journal of Haematology* 111, no. 2 (2023): 172–180.

58. Y. Hu, L. Zha, and K. Dai, "Regulation of Mitochondria on Platelet Apoptosis and Activation," *Zhongguo Shi Yan Xue Ye Xue Za Zhi* 31, no. 3 (2023): 816–822.

59. S. Herzig and R. J. Shaw, "AMPK: Guardian of Metabolism and Mitochondrial Homeostasis," *Nature Reviews. Molecular Cell Biology* 19, no. 2 (2018): 121–135.

60. S. Jager, C. Handschin, J. St-Pierre, et al., "AMP-Activated Protein Kinase (AMPK) Action in Skeletal Muscle via Direct Phosphorylation of PGC-1alpha," *Proceedings of the National Academy of Sciences of the United States of America* 104, no. 29 (2007): 12017–12022.

61. S. Yang and G. Lian, "ROS and Diseases: Role in Metabolism and Energy Supply," *Molecular and Cellular Biochemistry* 467, no. 1–2 (2020): 1–12.

62. Y. Chu, E. Dai, Y. Li, et al., "Pan-Cancer T Cell Atlas Links a Cellular Stress Response State to Immunotherapy Resistance," *Nature Medicine* 29, no. 6 (2023): 1550–1562.

63. N. Kozhukhar and M. F. Alexeyev, "35 Years of TFAM Research: Old Protein, New Puzzles," *Biology-Basel* 12, no. 6 (2023): 823.

64. M. Fischer, G. R. Bantug, S. Dimeloe, et al., "Early Effector Maturation of Naive Human CD8(+) T Cells Requires Mitochondrial Biogenesis," *European Journal of Immunology* 48, no. 10 (2018): 1632–1643.

65. L. Zhang, R. Ni, J. Li, et al., "Dioscin Regulating Bone Marrow Apoptosis in Aplastic Anemia," *Drug Design, Development and Therapy* 16 (2022): 3041–3053.

66. X. Dai, Q. Li, T. Li, et al., "The Interaction Between C/EBPbeta and TFAM Promotes Acute Kidney Injury via Regulating NLRP3 Inflammasome-Mediated Pyroptosis," *Molecular Immunology* 127 (2020): 136–145.

67. N. Rumpel, G. Riechert, and J. Schumann, "miRNA-Mediated Fine Regulation of TLR-Induced M1 Polarization," *Cells* 13, no. 8 (2024): 701.

68. M. Gao, X. Meng, Y. Cui, et al., "Role of Macrophage TLR4 Expression in the Immunopathogenesis of Severe Aplastic Anemia," *Journal of Clinical Laboratory Analysis* 39, no. 12 (2025): e70055.

69. R. Fu, Y. Meng, Y. Wang, et al., "The Dysfunction of Platelets in Paroxysmal Nocturnal Hemoglobinuria," *Thrombosis Research* 148 (2016): 50–55.

70. S. Deng, Q. Deng, Y. Zhang, et al., "Non-Platelet-Derived CXCL4 Differentially Regulates Cytotoxic and Regulatory T Cells Through CXCR3 to Suppress the Immune Response to Colon Cancer," *Cancer Letters* 443 (2019): 1–12.

71. D. Cruceriu, O. Baldasici, O. Balacescu, et al., "The Dual Role of Tumor Necrosis Factor-Alpha (TNF-Alpha) in Breast Cancer: Molecular Insights and Therapeutic Approaches," *Cellular Oncology (Dordrecht)* 43, no. 1 (2020): 1–18.

72. L. Hu, W. Huang, B. Liu, and E. A. Eklund, "In Fanconi Anemia, Impaired Accumulation of Bone Marrow Neutrophils During Emergency Granulopoiesis Induces Hematopoietic Stem Cell Stress," *Journal of Biological Chemistry* 300, no. 8 (2024): 107548.

73. H. Min, E. Montecino-Rodriguez, and K. Dorshkind, "Effects of Aging on the Common Lymphoid Progenitor to Pro-B Cell Transition," *Journal of Immunology (Baltimore, Md.: 1950)* 176, no. 2 (2006): 1007–1012.

74. Y. Zeng and E. Katsanis, "The Complex Pathophysiology of Acquired Aplastic Anaemia," *Clinical and Experimental Immunology* 180, no. 3 (2015): 361–370.

75. M. Obaid, S. M. N. Udden, P. Alluri, and S. S. Mandal, "LncRNA HOTAIR Regulates Glucose Transporter Glut1 Expression and Glucose Uptake in Macrophages During Inflammation," *Scientific Reports* 11, no. 1 (2021): 232.

76. S. Dahariya, S. Raghuwanshi, V. Thamodaran, S. R. Velayudhan, and R. K. Gutti, "Role of Long Non-Coding RNAs in Human-Induced Pluripotent Stem Cells Derived Megakaryocytes: A p53, HOX Antisense Intergenic RNA Myeloid 1, and miR-125b Interaction Study," *Journal of Pharmacology and Experimental Therapeutics* 384, no. 1 (2023): 92–101.

77. Q. Yao, X. He, J. Wang, et al., "DLEU2/EZH2/GFI1 Axis Regulates the Proliferation and Apoptosis of Human Bone Marrow Mesenchymal Stem Cells," *Critical Reviews in Eukaryotic Gene Expression* 34, no. 3 (2024): 61–71.

Supporting Information

Additional supporting information can be found online in the Supporting Information section. **Figure S1:** Gene level and related protein expression. (A, B) Horizontal bar charts, UMAP plots illustrating the upregulation of certain genes and protein expression before and after using MOFA. (C) UMAP plot displaying the gene and protein expression levels across all groups. **Figure S2:** Increased Mitochondrial Energy Metabolism Signaling Pathway/TFAM Expression in T Cells in BMF. (A) Violin plots illustrating the enriched expression of different signaling pathway proteins in various cell types. (B) Heatmaps demonstrating the enriched expression of different signaling pathway proteins in various TNK cells. C: Heatmaps displaying the enriched expression of different signaling pathway proteins in various macrophages. **Figure S3:** Characteristics of Hematopoietic Progenitor Cells (HSPCs) in BMF. (A) UMAP plot showing different subtypes of HSPCs in four samples/groups. (B) UMAP plot displaying distinct subtypes of HSPCs across various samples/groups. (C) Bar chart illustrating the proportion of cells belonging to specific HSPCs subtypes in different samples/groups. (D) Bubble heatmap displaying marker genes for various HSPCs subtypes. The size of the bubble indicates the proportion of the expressed subtype, colored according to z-score. (E) Bubble heatmap demonstrating signaling pathways among different HSPCs subtypes. The size of the bubble represents the proportion of the expressed subtype, colored according to *p*_val_adj. (F) Word cloud illustrating enriched biological processes in samples/groups. The size of the font represents the frequency of enrichment. (G) Heatmap displaying the enrichment level of differentially expressed genes (DEGs) in different HSPCs subtypes across various samples/groups. These numbers represent the enrichment scores. **Figure S4:** Neutrophils are Significantly Reduced in BMF. (A) UMAP plot showing different neutrophil subtypes in different samples/groups. (B) UMAP plot showing different neutrophil subtypes in different samples/groups. (C) Bar chart showing the cell proportion of specified neutrophil subtypes in different samples/groups. (D) Bubble heatmap showing marker genes of different neutrophil subtypes. The size of the dots represents the proportion of expressing neutrophil subtypes, colored according to zscore. (E) Volcano plot showing marker genes of 6 neutrophil subtypes. (F) Bubble heatmap showing signaling pathways between different neutrophil subtypes. The size of the dots represents the proportion of expressing neutrophil subtypes, colored according to *p*_val_adj. (G) Word cloud diagram showing enriched biological processes in samples/groups. The font size represents the enrichment frequency. (H) Heatmap showing the enrichment degree of differentially expressed genes (DEGs) in different neutrophil subtypes in different samples/groups. These numbers represent the enrichment scores. **Figure S5:** Characteristics of B Cells/Plasma Cells in BMF. (A) UMAP plot showing different B subtypes in different samples/groups. (B) UMAP plot showing different B subtypes in different samples/groups. (C) Bar chart showing the proportion of cells of a specified B subtype in different samples/groups. (D) Violin plot showing marker genes of different B subtypes. (E) UMAP plot showing marker genes of different B subtypes. (F) Bubble heatmap showing signaling pathways of different B subtypes. The size of the dots represents the proportion of B subtypes expressed, colored according to *p*_val_adj. (G) Heatmap showing signaling pathways compared among different B subtypes in various groups. **Figure S6:** Long Non-Coding RNA (lncRNA). (A) Bubble heatmap illustrating the enriched long non-coding genes across different samples. The size of the dots represents the expression ratio, colored based on z-score. **Table S1:** List of Abbreviations.